DOI: https://doi.org/10.24425/amm.2025.156251

M. NEDELJKOVIĆ<sup>©1\*</sup>, S. MLADENOVIĆ<sup>©1</sup>, V. ĆOSOVIĆ<sup>©2</sup>, I. MARKOVIĆ<sup>©1</sup>, J. PETROVIĆ<sup>©1</sup>, U. STAMENKOVIĆ<sup>©1</sup>

# MICROSTRUCTURE, WETTABILITY, AND THERMAL PROPERTIES OF SINTERED Sn-0.7Cu EUTECTIC ALLOY REINFORCED WITH GRAPHENE NANOSHEETS

In this study, various contents of graphene nanosheets (GNS) were successfully incorporated into Sn-0.7Cu base alloy by powder metallurgy (PM) technique to form Sn-0.7Cu-xGNS composite materials. The synthesis process included mixing and mechanical alloying, compacting and sintering. The effects of GNS on the microstructure, wettability, microhardness and melting properties were investigated. Optical and scanning electron microscopy (SEM) with energy-dispersive spectroscopy (EDS) revealed that the distribution of GNS in the solder matrix became more evident as the content of GNS increased. The reinforcement particles were homogeneously distributed at the grain boundaries, resulting in a finer  $\beta$ -Sn structure. The melting temperatures of the synthesized composites, determined by differential scanning calorimetry (DSC), are slightly higher than those of the Sn-0.7Cu base alloy. Incorporating GNS into the Sn-0.7Cu matrix enhanced microhardness up to 15.65% and reduced the contact angle between the composite solder and copper substrate up to 48.6%, significantly improving wettability.

Keywords: Mechanical alloying; powder metallurgy; graphene nanosheets; composites

#### 1. Introduction

The electronics industry continuously adapts to the demands of the latest generation of electronic devices, with advancements in electronics being paralleled by developments in soldering technology. Solder materials, which serve as metal fillers or interlayers, are used to connect various components in electrical devices or circuits, playing a crucial role in ensuring reliable solder joints. Historically, Pb-containing solders were commonly used in the electronics industry. Lead poses a potential risk to human health and the environment and should be eliminated [1-4]. Recognizing these facts, several nations have begun to take necessary safety measures, such as establishing rules limiting or prohibiting the use of lead in electronics. The European Union (EU) adopted two directives: WEEE (Waste Electrical and Electronic Equipment) and RoHS (Restriction of the Use of Certain Hazardous Substances) [5,6]. The production of lead-free solder alloys has become a great challenge for many researchers. New solder materials need to satisfy certain requirements: low melting temperature, great wettability, and good mechanical and electrical properties. Hence, Sn-based lead-free solders, such as Sn-Ag, Sn-Bi, Sn-Cu, Sn-In, Sn-Sb, Sn-Zn, and Sn-Ag-Cu have emerged as promising alternatives

to Sn-Pb solders [7-10]. These solder alloys are also used as a matrix to make composite solder materials.

Composite solder materials are improved compared to solder alloys. There are several methods for adding reinforcements to these solders, and the most commonly used technique is the PM method. Certain researchers used various types of nanoparticles to modify lead-free solders, including metal particles (such as Al, Co, Ni, Mo, etc.) and non-metals, including different allotropic forms of carbon, such as fullerenes (FNS), graphene nanosheets (GNS), carbon nanotubes (CNT), singlewalled carbon nanotubes (SWCNT), and multi-walled carbon nanotubes (MWCNT) [11,12]. The earliest discovered allotropic form of carbon is graphite, which has a layered structure, with one of the layers being a modification known as graphene. Graphene is a two-dimensional (2D) atomic crystal with a thickness of one atom. It consists of carbon atoms arranged in a honeycomb hexagonal  $sp^2$  hybridized crystal structure. Carbon atoms in the grid are connected by strong covalent bonds [13]. For the production of nanomaterials, GNS are most frequently used. They are one-dimensional (1D) nanomaterials formed by etching or shaping graphene in one direction, consisting of several compressed single layers of graphene. Their thickness ranges from 3 to 30 nm, with a length of several micrometers [14,15].

Corresponding author: mnedeljkovic@tfbor.bg.ac.rs



UNIVERSITY OF BELGRADE – TECHNICAL FACULTY IN BOR, 19210 BOR, SERBIA

<sup>&</sup>lt;sup>2</sup> UNIVERSITY OF BELGRADE – INSTITUTE OF CHEMISTRY, TECHNOLOGY AND METALLURGY, 11001 BELGRADE, SERBIA

The unique structural, electrical, thermal, and magnetic properties of these materials have attracted the attention of a large number of researchers [11,16-18].

Graphene has poor dispersibility in a metal matrix due to the presence of Van Der Waals forces, which leads to low wettability and a tendency to easily aggregate [13,19]. To improve the wettability between graphene nanoparticles and metal powders, mechanical alloying (MA) and mixing are the most used techniques for developing graphene-reinforced composite solders [20]. This method enables the production of new materials that are not obtainable by any other technique. Mechanical alloying represents a classical method for obtaining composite materials through solid-state alloying. This method involves cold welding, fracturing, and rewelding of powder particles in a high-energy ball mill [21].

Particle reinforcement is the primary strengthening technique in the production of lead-free composite solders. The addition of reinforcement particles aims to improve the mechanical properties and refine the microstructure of the solders [22]. Tsao et al. incorporated TiO2 nanoparticles into Sn-0.7Cu solder through mechanical alloying, leading to a finer microstructure and enhanced mechanical properties as the nanoparticle content increased [23]. Mohd Salleh and colleagues studied the impact of Si<sub>3</sub>N<sub>4</sub> particles on the properties of the Sn-0.7Cu solder alloy. The results showed that the microhardness of the composites increased by 25% compared to the base solder, while DSC measurements indicated that the presence of reinforcing Si<sub>3</sub>N<sub>4</sub> particles in the composites had a negligible effect on the melting temperature. Wettability testing using the sessile drop method revealed that the contact angle between the solder and the copper substrate decreased by 53% compared to the base alloy [24,25]. Zhong and Gupta reported that the addition of Al<sub>2</sub>O<sub>3</sub> particles in the Sn-0.7Cu alloy increased the microhardness and tensile strength of the composites as the reinforcement content increased. Microstructural analysis showed higher porosity with increasing Al<sub>2</sub>O<sub>3</sub> content [26]. According to the available literature, only Yang and his associates have studied the effect of different GNS contents (0.02, 0.050, 0.075, and 0.10 wt.%) on the properties of the Sn-0.7Cu base alloy. The results showed that with an increase in GNS content, the density of the composite solder did not change significantly, while the microhardness reached its highest value of 11.48 HV at 0.075 wt.% GNS. DSC results revealed that the reinforcing particles had no effect on the melting temperature of the tested samples. Incorporating GNS into the matrix alloy improved the wettability and shear strength of the composites. Their results indicated that the best properties (mechanical, electrical, and corrosion resistance) were achieved at 0.075 wt.% GNS [27,28].

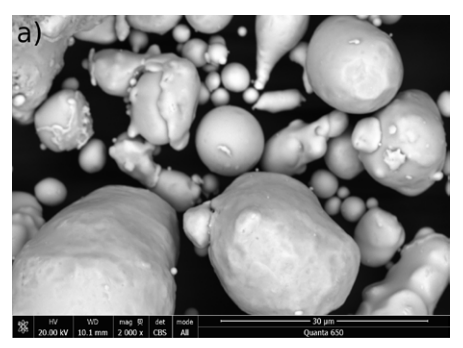
Since there is limited data on sintered Sn-0.7Cu-xGNS composite materials, this study investigates the effect of various GNS contents, which have not been previously studied in the Sn-0.7Cu base alloy, on the microstructure, wettability, microhardness, and melting point. The reinforced composites were produced using the PM technique. Mechanical alloying, cold pressing, and conventional sintering were applied to produce the composite samples. The obtained results were compared with those of the matrix alloy.

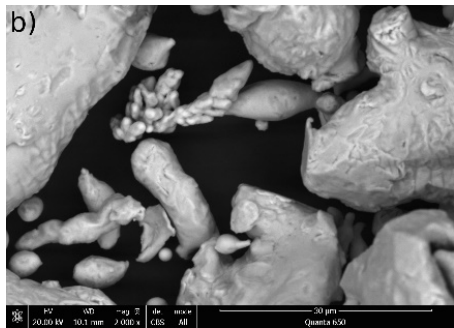
## 2. Experimental procedures

Elemental metal powders Sn (99.90% purity), Cu (99.96% purity), and GNS were used to produce Sn-0.7Cu alloy and Sn-0.7Cu-xGNS composite materials. Atomized Sn and Cu powders, with particle sizes up to 75  $\mu$ m, were purchased from MB "Wide Range Metals" in Lithuania. The GNS utilized in this study, with an average diameter of 5-10  $\mu$ m and a thickness of 3-5 layers, were supplied by "Shanghai Huirui Chemical Technology", China. SEM images of the powders used in this study, obtained with a "Quanta 650" SEM microscope, are presented in Fig. 1.

The Sn-0.7Cu-xGNS composite materials (with x = 0; 0.02; 0.04; 0.06; 0.08 and 0.1 wt.% GNS) were produced using the PM technique. First, the Sn and Cu powders were weighed separately in a specific ratio to form the Sn-0.7Cu base powder, and then mixed. The mixing process was performed with a "Turbula T2F" three-axis mixer at a speed of 50 rpm for 30 hours, without using balls or process control agents. Subsequently, the matrix powder and GNS were mechanically alloyed in a high energy planetary ball mill "FRITSCH Planetary Ball Mill P-7". Mechanical alloying was conducted at a speed of 100 rpm for 3 hours. The balls and the cup were made of tungsten carbide and the ball-to-powder ratio of 6:1 was utilized.

Each mixture was compacted using a "Mohr-Federhaff-Losenhausen" hydraulic press under a pressure of 300 MPa at room temperature to produce green compacts with a diameter of 12.7 mm. The green compacts were conventionally sintered





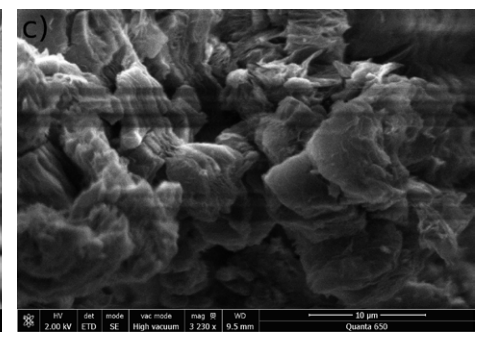


Fig. 1. SEM image of elemental powders (a) Sn; (b) Cu; (c) GNS

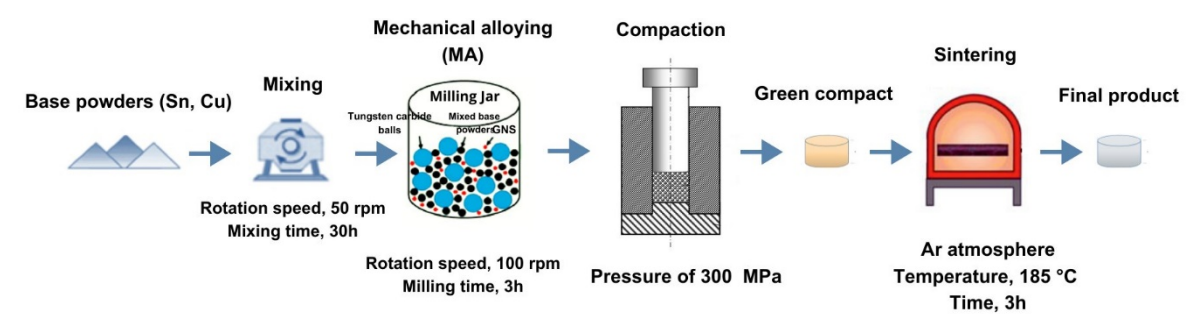


Fig. 2. Schematic illustration of production composite materials

in an inert argon atmosphere at 185°C for 3 hours. Fig. 2 provides a schematic illustration of the process for obtaining composite materials using the PM method.

The microstructural analysis of the sintered composite samples was performed using a combination of optical microscopy and SEM equipped with an EDS. After standard metallographic preparation by grinding and wet polishing, the samples were etched with a solution of (2 mL HCl + 100 mL of 95% methanol) according to ASTM E3 [29] and ASTM E407 standards [30]. The "Reichert MeF2" optical microscope was used for metallographic analysis, and the "Tescan Vega 3 LMU" SEM equipped with an EDS "Oxford Instruments X-act" was employed for microstructure observations and determination of the chemical compositions of the samples, including the presence and distribution of reinforcement particles. The average grain size was determined using ImageJ software.

The wettability of solder is an important factor that determines the quality of the bond between the solder and the substrate. Determination of solder wettability often involves measuring the contact angle ( $\theta$ ). Fig. 3 shows a correlation between the contact angle and surface tensions, which may be determined using the Young Eq. (1) [31,32]:

$$\cos\theta = \frac{\gamma_{sg} - \gamma_{ls}}{\gamma_{lg}} \tag{1}$$

where  $\gamma_{sg}$  is the surface tension between solid and gas,  $\gamma_{lg}$  is the surface tension between liquid solder and gas,  $\gamma_{ls}$  is the surface tension between liquid solder and solid, and  $\theta$  is the contact angle.

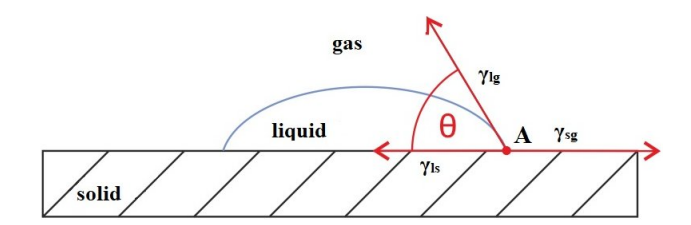


Fig. 3. The contact angle of a drop of liquid metal on a solid substrate adopted from the literature [31,32]

Copper substrates (20×20×1 mm) were polished with silicon-carbide paper to achieve a smooth surface. The prepared substrates were then dipped into acetone for 1 minute to remove oil and immersed in a hydrochloric acid solution to eliminate the oxide layer. Subsequently, cylindrical samples with a diameter of 3 mm and a height of 3 mm, weighing 0.2 g, were placed at the center of the substrate. The solder flux RMA223 was used to prevent oxide formation during soldering. The samples, along with the substrates, were heated to 250°C on a hot plate in air. A cross-section of the solders was observed using an OM, and the contact angle was measured using ImageJ software. Additionally, SEM-EDS analysis was performed to investigate the microstructure of the solders and solder joints after the soldering process. Fig. 4 shows different steps during the contact angle measurement.

The Vickers method was used to determine the microhardness of the sintered composite materials, according to the ASTM E384 standard [33]. Measurements were made on the "PMT-3" Vickers microhardness tester. A force of 0.5 N was applied, with

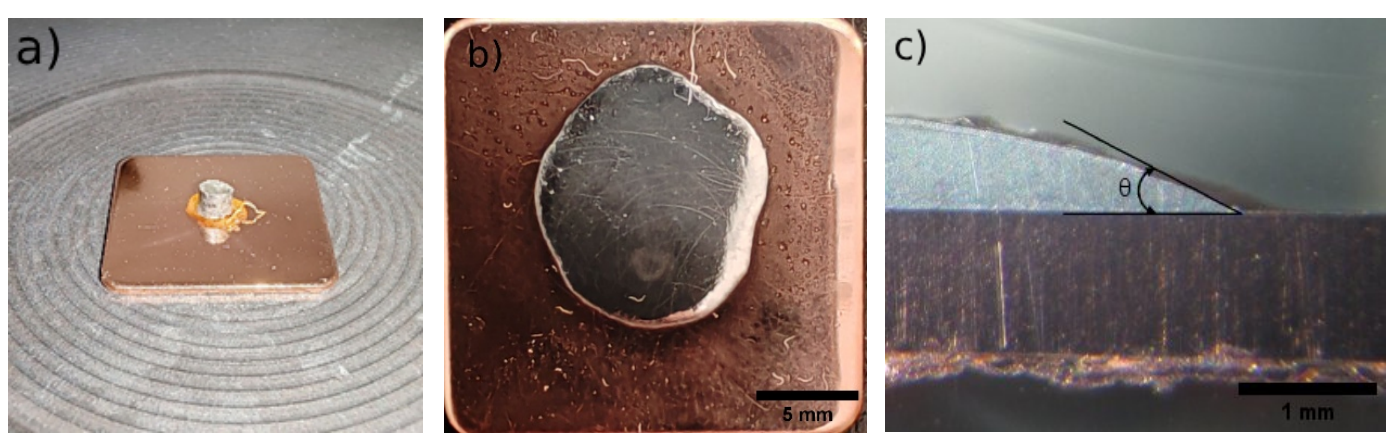


Fig. 4. Measuring process for the contact angle (a) sintered sample at Cu substrate; (b) after soldering; (c) cross-section of the molten droplet on Cu substrate

a load duration of 15 seconds. The procedure was conducted six times, and the average value was calculated.

To determine the melting point of the sintered composite materials TGA-DSC/DTA simultaneous thermal analyzer "TA Instruments SDT Q600" was used. Samples weighing approximately 10-20 mg, were heated from 30°C to 350°C at a heating rate of 10°C/min in a protective nitrogen atmosphere.

#### 3. Results and discussion

Microstructure research is essential for the development of solder alloys, since it can be used for determine the properties of solders and solder joints. The samples were characterized using SEM-EDS analysis to investigate the microstructure, identify microconstituents, and determine their chemical composition. EDS analysis confirmed the presence of intermetallic phases and reinforcing particles distributed along the grain boundaries.

Fig. 5 shows the SEM microphotographs of the investigated composites with different content of GNS. It can be seen that the addition of reinforcement particles significantly contributes to the reduction of the grain size, which was confirmed measuring the average grain size (Fig. 6).

Acording to Fig. 5 the presence of GNS in the composites with lower content of GNS (up to  $0.04 \, \text{wt.\%}$ ) is barely noticeable. At higher content (from  $0.06 \, \text{wt.\%}$  to  $0.10 \, \text{wt.\%}$ ), its presence becomes more evident in the microstructures. The GNS are mainly distributed along the grain boundaries (indicated with

arrows). Yang et al. observed that as the GNS content exceeded 0.08 wt.%, the GNS tended to agglomerate along the grain boundaries [27].

The average grain size continuously decreased from 23.69 µm to 13.18 µm, as the GNS content increased. The Sn-0.7Cu-0.10GNS composite has the finest microstructure with approximately 44.37% lower grain size than the Sn-0.7Cu alloy. The incorporation of GNS into the base matrix results in a grain refinement. The microstructure of Sn-0.7Cu-xGNS composites is more uniform and finer than the Sn-0.7Cu base alloy. According to this fact, it can be assumed that, on one hand, GNS act as centers of heterogeneous nucleation leading to grain refinement, while on the other hand, the higher the GNS content, the more significant the barrier effect that prevents grain growth. Similar results were also reported by Yang et al. in their studies [27].

The EDS results of Sn-0.7Cu-0.10GNS composite are shown in Fig. 7. The presence of the chemical elements tin, copper and carbon (C) has been determined. During the sintering phase of the PM method, the green compacts were heated to  $185^{\circ}$ C. This temperature enabled diffusion between particle surfaces, which was sufficient to densify the green compacts but insufficient to form a eutectic phase. The distribution of the intermetallic phase in the sintered Sn-0.7Cu-0.10GNS alloy appears to be heterogeneous. The primary matrix consists of nearly pure tin (99.3%). According to the phase diagram [34], the formation of the  $\text{Cu}_6\text{Sn}_5$  intermetallic compound within the tin matrix would be expected. EDS analysis in Fig. 7 (spectrum 1 and 4) confirms the presence of an intermetallic compound based

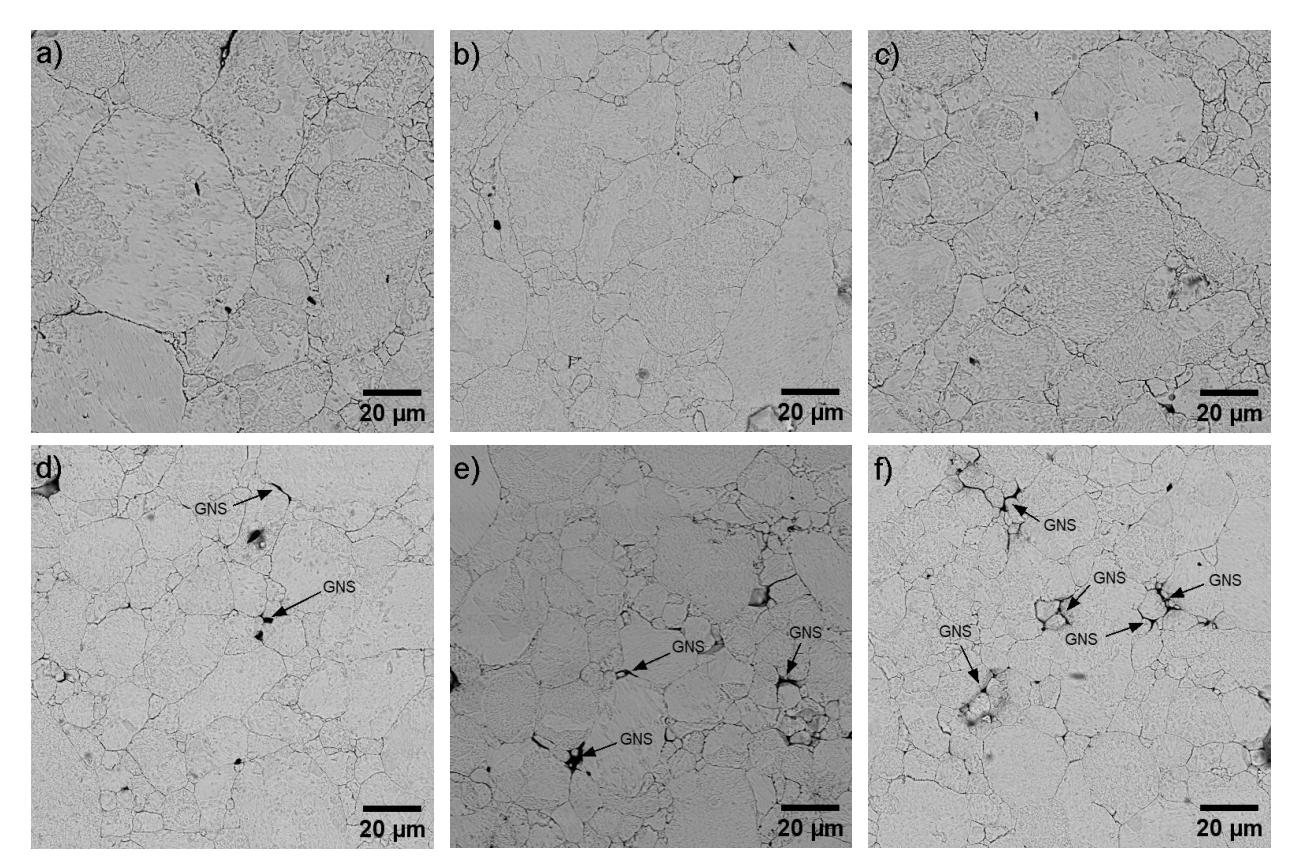
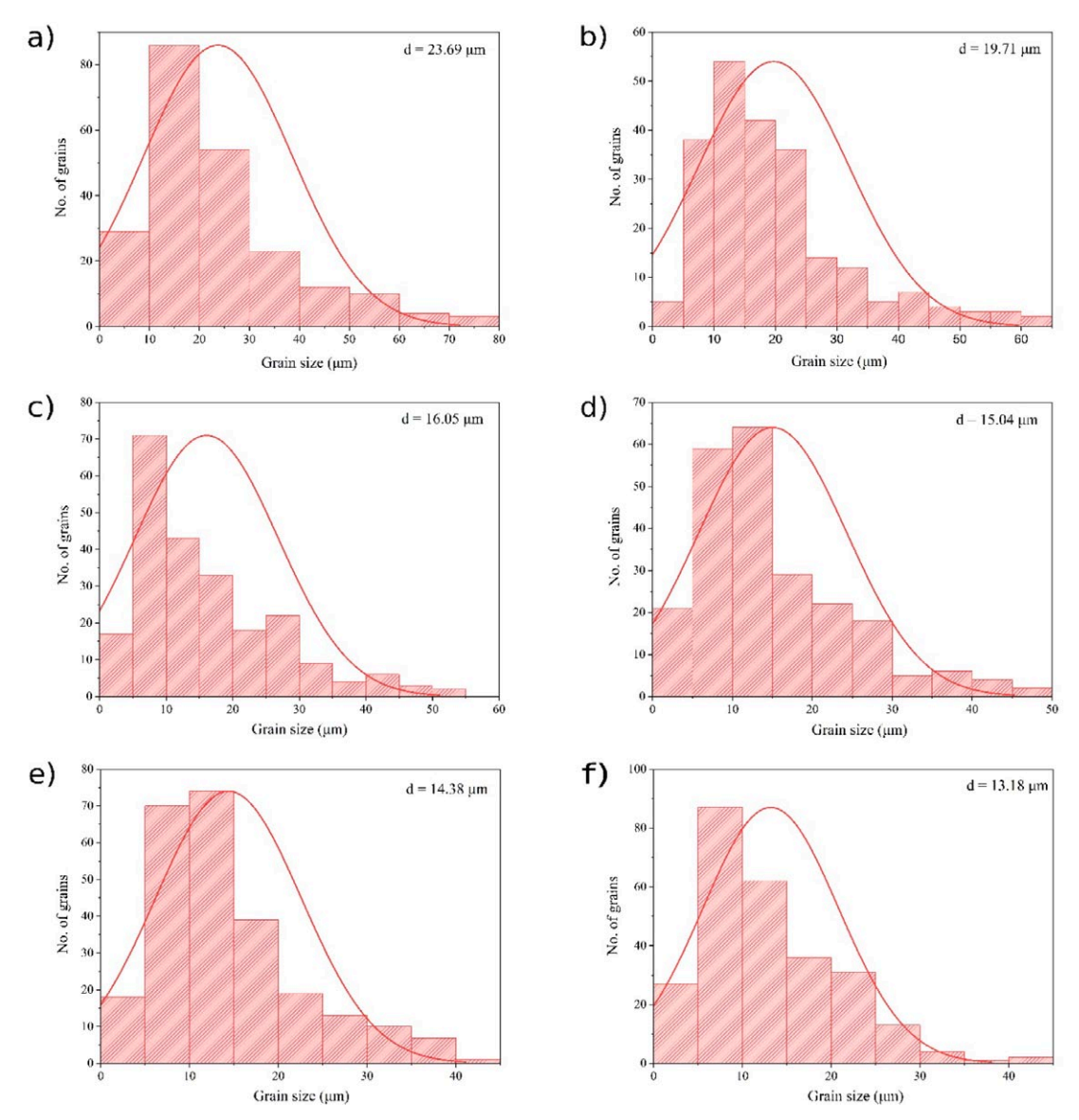


Fig. 5. SEM microphotographs of the Sn-0.7Cu-xGNS samples; (a) Sn-0.7Cu; (b) Sn-0.7Cu-0.02GNS; (c) Sn-0.7Cu-0.04GNS; (d) Sn-0.7Cu-0.06GNS; (e) Sn-0.7Cu-0.08GNS; (f) Sn-0.7Cu-0.10GNS



 $Fig.\ 6.\ Grain\ size\ distribution\ in\ the\ PM\ samples\ (a)\ Sn-0.7Cu; (b)\ Sn-0.7Cu-0.02GNS; (c)\ Sn-0.7Cu-0.04GNS; (d)\ Sn-0.7Cu-0.06GNS; (e)\ Sn-0.7Cu-0.08GNS; (f)\ Sn-0.7Cu-0.10GNS$ 

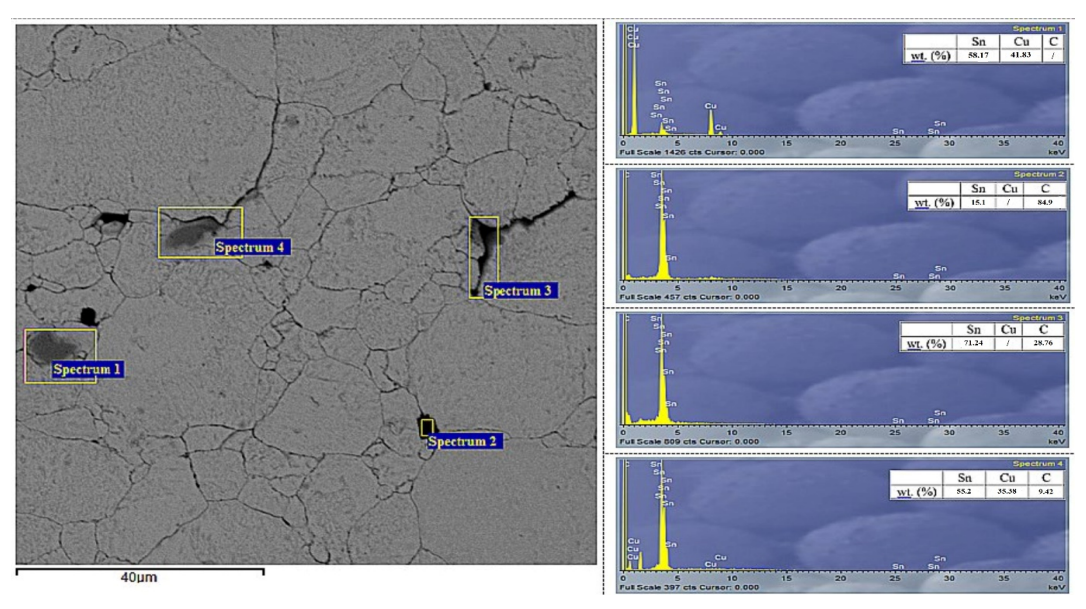


Fig. 7. The EDS chemical composition analysis of the Sn-0.7Cu-0.10GNS composite

on Sn and Cu, which, based on its stoichiometric ratio, can be identified as the  $Cu_6Sn_5$  phase. Additionally, the presence of carbon (spectrum 2, 3 and 4) indicates that GNS is distributed along the grain boundaries. These results align with findings previously reported by Huang et al. and Salleh et al. [35,36].

To identify the distribution of the presented elements in the composite, element distribution maps were performed (Fig. 8).

In the micrograph in Fig. 8a, grain boundaries can be observed, where graphene particles has agglomerated. Figs. 8(b-d) illustrates the distribution of Sn, Cu, and C, respectively in the investigate sample. Even though GNS has agglomerated on the grain boundaries, a homogeneous distribution of carbon throughout the structure can also be observed (Fig. 8d). This indicates the successful mechanical alloying of GNS in the matrix.

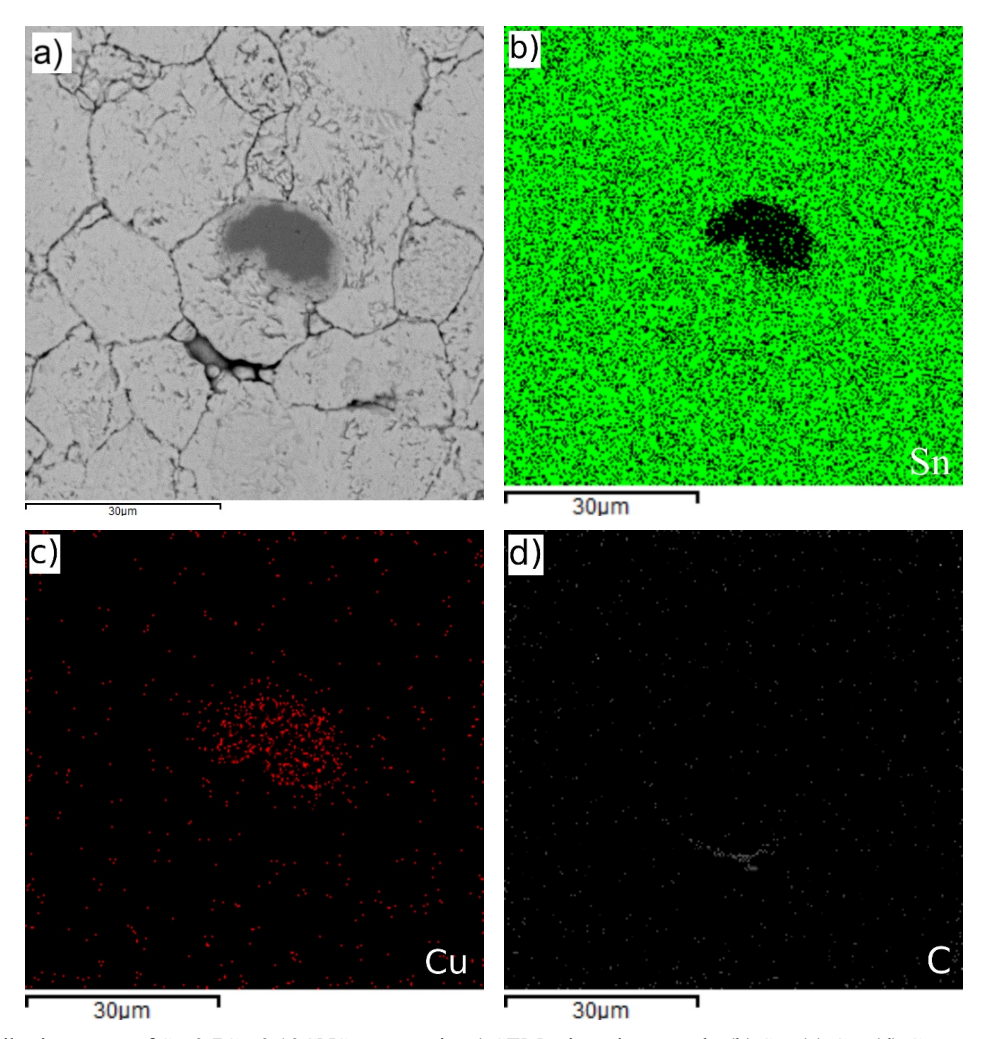


Fig. 8. Element distribution maps of Sn-0.7Cu-0.10GNSs composite a) SEM microphotograph; (b) Sn; (c) Cu; (d) C

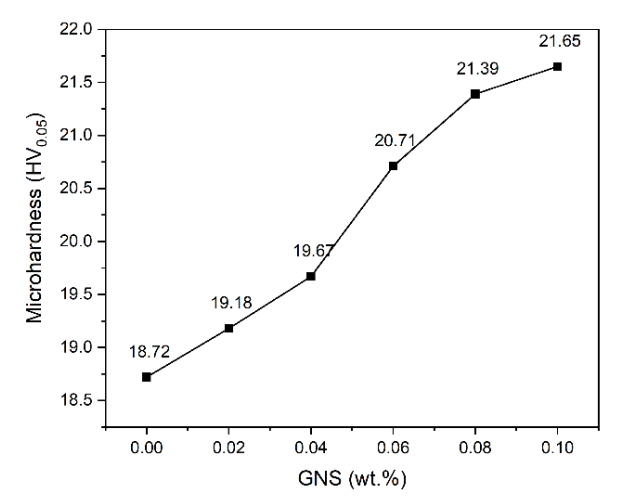


Fig. 9. Microhardness of Sn-0.7Cu-xGNS samples

Microhardness testing is a commonly used method for characterizing the mechanical properties of solid surfaces. The microhardness of a solder alloy is affected by dislocation movement, as well as grain growth and the microstructure refinement. Fig. 9 shows the changes in microhardness of the sintered samples as a function of the weight content of GNS.

It can be noticed that the microhardness of the obtained Sn-0.7Cu-xGNSs composite samples continually increases with the increasing amount of GNS. A similar result was reported by Yin and colleagues [37]. Sn-0.7Cu base alloy has a microhardness of 18.72 HV $_{0.05}$ , while composite with a GNS content of 0.10 wt.% has a microhardness of 21.65 HV $_{0.05}$ , which is approximately 15.65% higher than the Sn-0.7Cu alloy. The increase in microhardness is mainly attributed to the uniform distribution of GNS and the microstructure refinement induced

by reinforcement particles. During the sintering process, Sn-0.7Cu exhibits good fluidity, while GNS act as a hard second phase. The GNS are surrounded by the Sn-0.7Cu matrix and are pinned at the grain boundaries, as shown in Fig. 7. GNS are dispersed within the Sn-0.7Cu matrix (Fig. 8), contributing to dispersion strengthening. Additionally, a higher GNS content reduces interparticle spacing, making dislocation movement more difficult, which also leads to an increase in microhardness. A higher GNS content also increases stress due to the difference in the coefficient of thermal expansion between the matrix and the reinforcement [28]. These stresses cause the deformation of the crystal lattice of the metal matrix and the accumulation of dislocations, which is another factor contributing to the increase in microhardness.

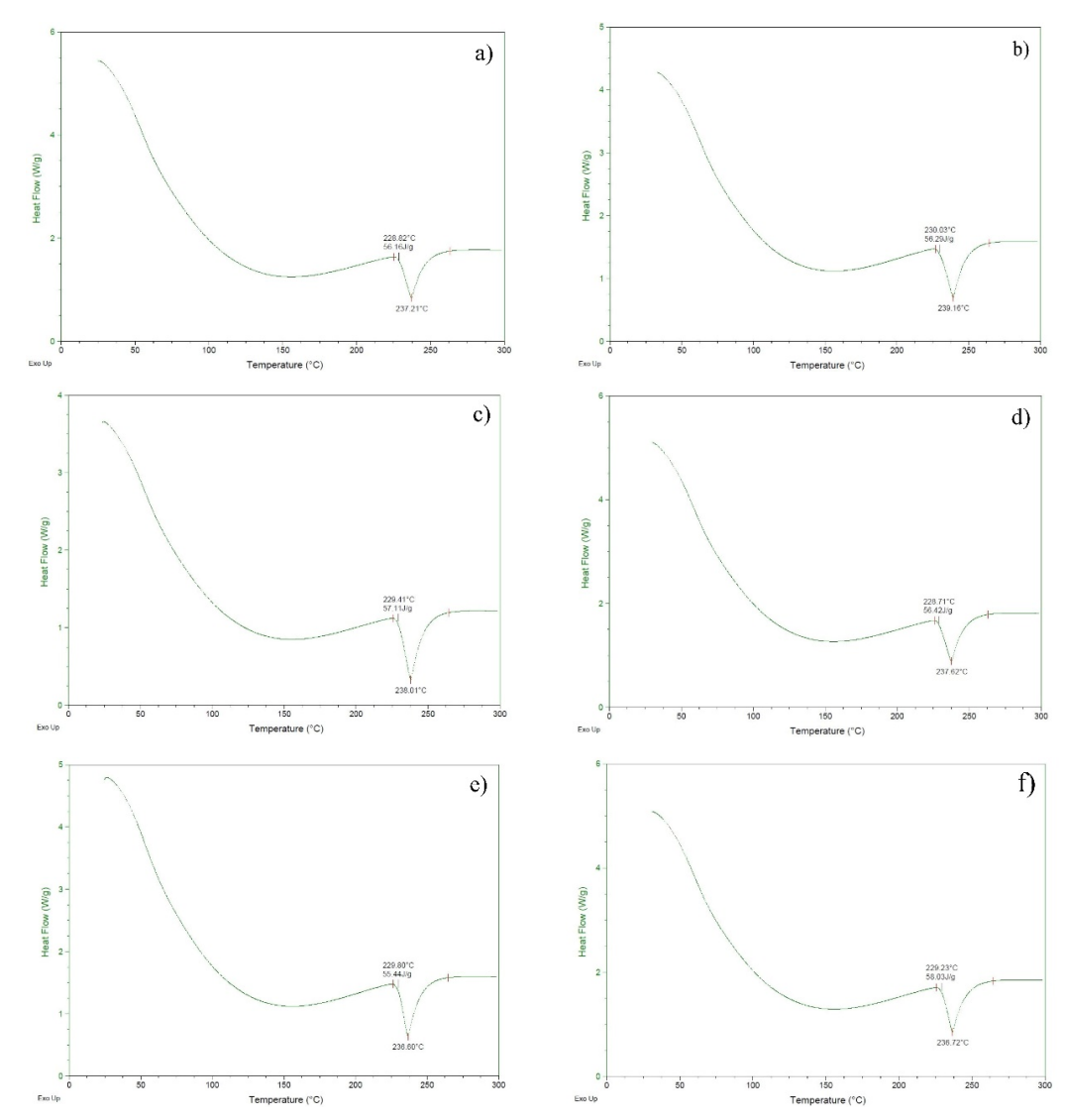
In the soldering process, the melting temperature plays a determining role. The identification of the characteristic temperatures of the phase transformations was performed according to the recommendations from the literature [34]. Fig. 10 illustrates the DSC curves of the sintered Sn-0.7Cu-xGNS samples. DSC heating curves for the six investigated samples exhibit an

endothermic peak at nearly the same temperature, corresponding to the eutectic reaction  $\beta$ -Sn +  $\eta$ -Cu<sub>6</sub>Sn<sub>5</sub>  $\rightarrow$  R.

The onset temperature of the first observed peak was identified as the eutectic reaction temperature, corresponding to the solidus temperature, whereas the peak temperature of the second thermal effect was considered the liquidus temperature [38]. The eutectic temperature of the Sn-0.7Cu base alloy obtained by DSC was 228.82°C which is slightly higher than the literature value of 227°C [34]. The melting properties of Sn-0.7Cu-xGNS alloys are summarized in TABLE 1.

TABLE 1 Melting properties of Sn-0.7Cu-xGNS alloys

Samples	$T_S$ (°C)	$T_L$ (°C)	ΔT (°C)
Sn-0.7Cu	228.82	237.21	8.39
Sn-0.7Cu-0.02GNS	230.03	239.16	9.13
Sn-0.7Cu-0.04GNS	229.41	238.81	9.40
Sn-0.7Cu-0.06GNS	228.71	237.62	8.91
Sn-0.7Cu-0.08GNS	229.80	236.60	6.80
Sn-0.7Cu-0.10GNS	229.23	236.72	7.49



 $Fig. \ 10. \ DSC \ heating \ curves \ (a) \ Sn-0.7 Cu-0.02 GNS; \ (c) \ Sn-0.7 Cu-0.04 GNS; \ (d) \ Sn-0.7 Cu-0.06 GNS; \ Sn-0.7 Cu-0.08 GNS, \ Sn-0.7 Cu-0.10 GNS; \ (d) \ Sn-0.7 Cu-0.06 GNS; \ Sn-0.7 Cu-0.08 GNS, \ Sn-0.7 Cu-0.08 GNS; \ (d) \ Sn-0.7 C$ 

Based on the results, it can be concluded that the presence of GNS in composite materials with a Sn-0.7Cu base alloy has a negligible effect on the eutectic and liquidus temperatures. The melting range ( $\Delta T$ ) for all tested samples is less than 10°C. Similar findings were published by Yang et al. in their study [27].

The wettability of Sn-0.7Cu-xGNS solders was characterized by measuring the contact angle. Fig. 11 presents the measured values of contact angle between the solders and Cu substrate. The results indicate that adding GNS enhances the wettability of composite solders. The base Sn-0.7Cu solder has a contact angle of 38.09°, while the composite solder with a GNS content of 0.10 wt.% has a contact angle of 19.59°, which is approximately 48.6% lower than the Sn-0.7Cu base solder.

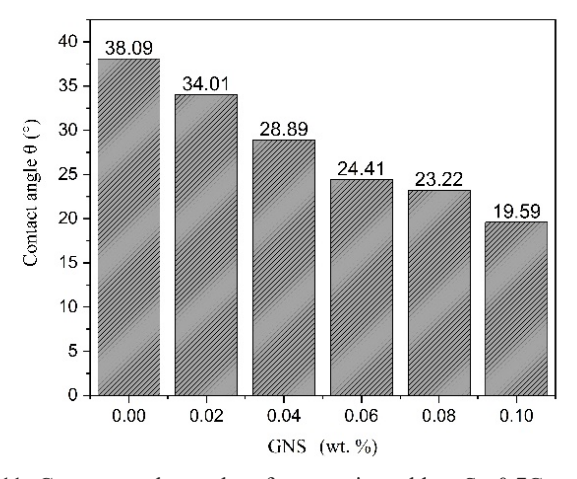


Fig. 11. Contact angle results of composite solders Sn-0.7Cu-xGNS on Cu substrate

According to the literature solders with  $\theta$  < 30° show very good wetting, with  $\theta$  = 30°-40° show good wetting,  $\theta$  = 40°-55° show acceptable wetting, while with  $\theta$  = 55°-70° show poor wetting, and  $\theta$  > 70° show very poor wetting [32]. Composites with higher GNS content then 0.02 wt.% show very good wetting.

Based on the obtained results, the following assumption was made. GNS are non-polar molecules with a hexagonal honeycomb lattice composed of carbon-carbon covalent bonds. When the GNS in the molten composite solder come into contact with the non-polar molecules in organic acids in the solder flux during soldering, the dispersion between the non-polar molecules of these compounds may occur. This reduces the interphase tension between the solder and the flux. Based on Young's Eq. (1), reducing the interpase tension lowers the contact angle, which improves the wettability of the composite solders. Similar results have been reported by Yin et al. and Liu et al. in their studies [37,39].

After the wettability test, the microstructure of the solders and the interfacial growth of intermetallic compounds at the solder/Cu interface were examined. Fig. 12 shows the corresponding SEM microstructures of the intermetallic layer after soldering process.

SEM-EDS analysis revealed that the matrix consists of a solid solution of  $\beta$ -Sn, along with a needle-like intermetallic phase Cu<sub>6</sub>Sn<sub>5</sub>, which is embedded within the  $\beta$ -Sn structure. It was observed that a typical wave-serrated Cu<sub>6</sub>Sn<sub>5</sub> intermetallic layer formed at the interface between the Sn-0.7Cu-xGNS solder and the Cu substrate after the soldering process. The thickness of the intermetallic layer was determined using ImageJ software.

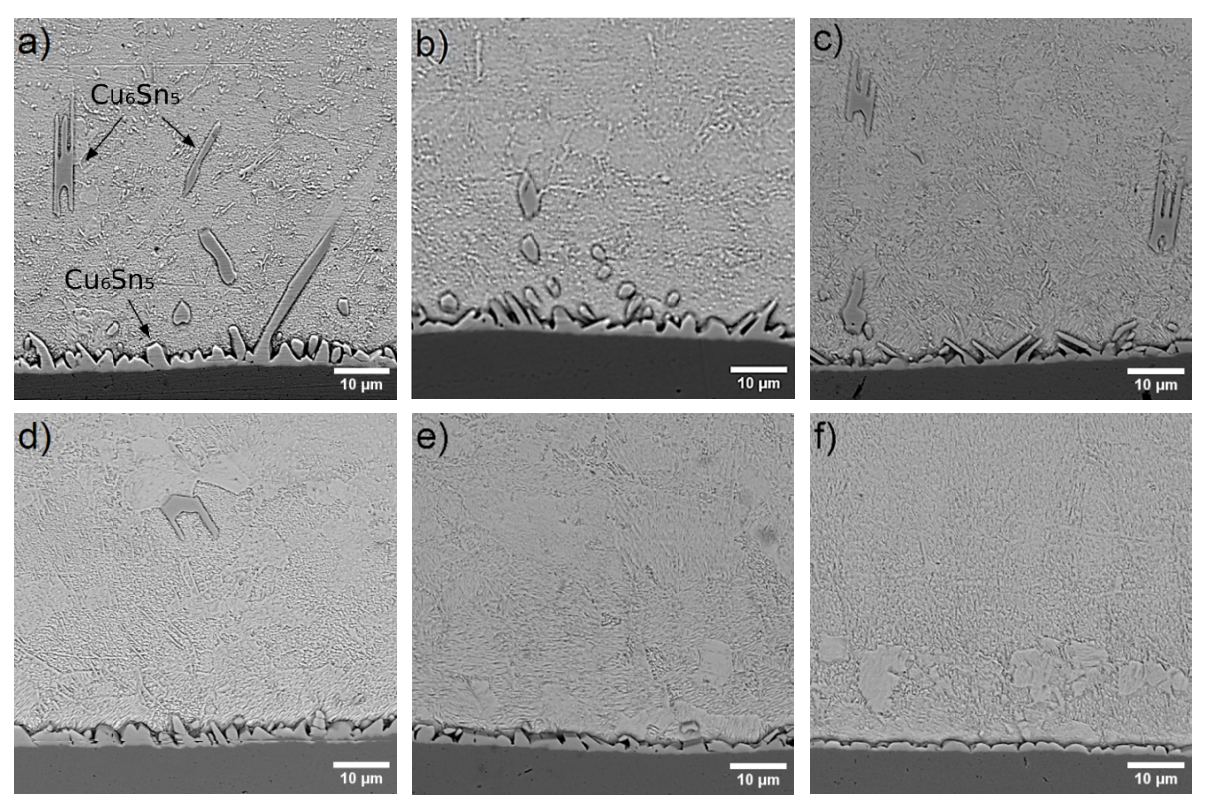


Fig.12. SEM micrographs of the intermetallic layer between Sn-0.7Cu-xGNS solders and Cu substrate (a) Sn-0.7Cu; (b) Sn-0.7Cu-0.02GNS; (c) Sn-0.7Cu-0.04GNS; (d) Sn-0.7Cu-0.06GNS; (e) Sn-0.7Cu-0.08GNS; (f) Sn-0.7Cu-0.10GNS

The results indicated that the thickness of the intermetallic layer decreased with increasing GNS content in the solder. The high specific surface area of GNS slows down the diffusion of metal atoms when added to the solder. GNS acts as a barrier to the diffusion of Cu and Sn atoms, leading to the formation of a thinner intermetallic layer. Additionally, due to its low density and tendency to agglomerate, GNS accumulates at the interface between the solder and the substrate, further restricting the diffusion of Cu atoms from the copper substrate. As a result, the reduced diffusion of Cu slows the formation of the intermetallic layer. Therefore, the presence of GNS in Sn-0.7Cu-xGNS composite solders inhibits the growth of intermetallic compounds at the solder/substrate interface. This finding aligns with reported results in the literature [40].

#### 4. Conclusions

In this study, Sn-0.7Cu-xGNS composite materials with x = 0; 0.02; 0.04; 0.06; 0.08 and 0.1 wt.% GNS were successfully synthesized by the PM technique. The conclusions can be summarized as follows:

- The synthesized composites have a more homogeneous and finer-grained microstructure compared to the Sn-0.7Cu base alloy. The GNS are mainly distributed along the grain boundaries, resulting in a finer β-Sn structure.
- The addition of GNS to the Sn-0.7Cu base alloy enhanced the microhardness of the composite material.
- There is no significant changes in the eutectic and liquidus temperatures of the composite materials compared to solder matrix.
- With increasing GNS content, the composite solders exhibit a reduced contact angle, improved wettability, and a thinner intermetallic layer at the solder/substrate interface compared to the Sn-0.7Cu base solder.

## Acknowledgments

The research presented in this paper was done with the financial support of the Ministry of Science, Technological Development and Innovation of the Republic of Serbia, with the funding of the scientific research work at the University of Belgrade, Technical Faculty in Bor, according to the contract with registration number 451-03-137/2025-03/200131 and the Ministry of Science, Technological Development and Innovation of Republic of Serbia (Contract No. 451-03-136/2025-03/200026).

### REFERENCES

[1] N.S.M. Zaimi, M.A.A.M. Salleh, M.M. Al Bakri Abdullah, M.I.I. Ramli, A Short Review on the Influence of Antimony Addition to the Microstructure and Thermal Properties of Lead-Free Solder Alloy. Arch. Metall. Mater. 68, 3, 981-986 (2023). DOI: https://doi.org/10.24425/amm.2023.145463

- [2] M.A.A.M. Salleh, M.H. Hazizi, Z.A. Ahmad, K. Hussin, K.R. Ahmad, Wettability, electrical and mechanical properties of 99.3Sn-0.7Cu/Si<sub>3</sub>N<sub>4</sub> novel lead-free nanocomposite solder. Adv. Mat. Res. 277, 106-111 (2011).
  - DOI: https://doi.org/10.4028/www.scientific.net/amr.277.106
- J. Shen, Y.C. Chan, Research advances in nano-composite solders.
   Microelectron. Reliab. 49 (3), 223-234 (2009).
   DOI: https://doi.org/10.1016/j.microrel.2008.10.004
- [4] K.J. Puttlitz, K.A. Stalter, Handbook of lead-free solder technology for microelectronic assemblies. CRC Press, Boca Raton 2004. DOI: https://doi.org/10.1201/9780203021484
- [5] S. Bogaert, M. Van Acoleyen, I. Van Tomme, L. De Smet, D. Fleet,
   R. Salado, Study on RoHS and WEEE Directives. By ARCADIS
   & RPA for the DG ENTR, European Commission. (2008).
- [6] A. Gyenes, A. Simon, P. Lanszki, Z. Gácsi, Effects of nickel on the microstructure and the mechanical properties of Sn-0.7Cu lead-free solders. Arch. Metall. Mater. 60 (2B), 1449-1454 (2015). DOI: http://dx.doi.org/10.1515/amm-2015-0151
- P. Fima, Surface tension and density of liquid Sn–Cu alloys. Appl. Surf. Sci. 257 (2), 468-471 (2010).
   DOI: http://dx.doi.org/10.1016/j.apsusc.2010.07.013
- [8] C.S. Hsi, C.T. Lin, T.C. Chang, M.C. Wang, M.K. Liang, Interfacial reactions, microstructure, and strength of Sn-8Zn-3Bi and Sn-9Zn-Al solder on Cu and Au/Ni (P) pads. Metall. Mater. Trans. A. 41, 275-284 (2010).
  DOI: http://dx.doi.org/10.1007/s11661-009-0109-6
- [9] L.R. Garcia, W.R. Osório, A. Garcia, The effect of cooling rate on the dendritic spacing and morphology of Ag<sub>3</sub>Sn intermetallic particles of a SnAg solder alloy. Mater. Design. 32 (5), 3008-3012 (2011). DOI: https://doi.org/10.1016/j.matdes.2010.12.046
- [10] C.M.L. Wu, D.Q. Yu, C.M.T. Law, L. Wang, Properties of lead-free solder alloys with rare earth element additions. Mater. Sci. Eng. R: Rep. 44 (1), 1-44 (2004).
  DOI: https://doi.org/10.1016/j.mser.2004.01.001
- [11] Y. Li, S. Yu, L. Li, S. Song, W. Qin, D. Qi, Y. Zhan, A review on the development of adding graphene to Sn-based lead-free solder. Metals. 13 (7), 1209 (2023). DOI: https://doi.org/10.3390/met13071209
- [12] M.B.K. Teja, A. Sharma, S. Das, K. Das, A review on nanodispersed lead-free solders in electronics: synthesis, microstructure and intermetallic growth characteristics. J. Mater. Sci. 57 (19), 8597-8633 (2022).
  DOI: https://doi.org/10.1007/s10853-022-07187-8
- [13] P. R. Wallace, The band theory of graphite. Phys. Rev. **71** (9), 622 (1947). DOI: https://doi.org/10.1103/PhysRev.71.622
- [14] Y. Huang, Z. Xiu, G. Wu, Y. Tian, P. He, Sn–3.0 Ag–0.5 Cu nanocomposite solders reinforced by graphene nanosheets. J. Mater. Sci.-Mater. El. 27, 6809-6815 (2016).
  DOI: https://doi.org/10.1007/s10854-016-4631-1
- [15] D. Tošić, Sinteza i karakterizacija grafenskih nanotraka. PhD thesis, University in Belgrade, Belgrade, Serbia (2016).
- [16] N.O. Weiss, H. Zhou, L. Liao, Y. Liu, S. Jiang, Y. Huang, X. Duan, Graphene: an emerging electronic material. Adv. Mater. 24 (43), 5782-5825 (2012). DOI: https://doi.org/10.1002/adma.201201482

- [17] A.H. Castro Neto, F. Guinea, N.M. Peres, K.S. Novoselov, A.K. Geim, The electronic properties of graphene. Rev. Mod. Phys. 81 (1), 109-162 (2009). DOI: https://doi.org/10.1103/revmodphys.81.109
- [18] R. Ranjan, V. Bajpai, Graphene-based metal matrix nanocomposites: Recent development and challenges. J. Compos. Mater. 55 (17), 2369-2413 (2021).
   DOI: https://doi.org/10.1177/0021998320988566
- [19] E.A. Kim, A.C. Neto, Graphene as an electronic membrane.
   Europhys. Lett. 84 (5), 57007 (2008).
   DOI: https://doi.org/10.1209/0295-5075/84/57007
- [20] A.K. Geim, K.S. Novoselov, The rise of graphene. Nat. Mater. 6
   (3), 183-191 (2007).
   DOI: https://doi.org/10.1038/nmat1849
- [21] A.K. Geim, Graphene: status and prospects. Science. 324 (5934), 1530-1534 (2009).
   DOI: https://doi.org/10.1126/science.1158877
- [22] L. Xu, X. Chen, H. Jing, L. Wang, J. Wei, Y. Han, Design and performance of Ag nanoparticle-modified graphene/SnAgCu lead-free solders. Mat. Sci. Eng. A-Struct. 667, 87-96 (2016). DOI: https://doi.org/10.1016/j.msea.2016.04.084
- [23] L.C. Tsao, C.H. Huang, C.H. Chung, R.S. Chen, Influence of TiO<sub>2</sub> nanoparticles addition on the microstructural and mechanical properties of Sn-0.7Cu nano-composite solder. Mat. Sci. Eng. A-Struct. 545, 194-200 (2012). DOI: https://doi.org/10.1016/j.msea.2012.03.025
- [24] M.M. Salleh, A.M. Al Bakri, M.H. Zan, F. Somidin, N.F.M. Alui, Z.A. Ahmad, Mechanical properties of Sn–0.7Cu/Si<sub>3</sub>N<sub>4</sub> lead-free composite solder. Mat. Sci. Eng. A-Struct. 556, 633-637 (2012). DOI: https://doi.org/10.1016/j.msea.2012.07.039
- [25] M.M. Salleh, A.M. Al Bakri, H. Kamarudin, M. Bnhussain, F. Somidin, Solderability of Sn-0.7Cu/Si<sub>3</sub>N<sub>4</sub> lead-free composite solder on Cu-substrate. Physcs. Proc. 22, 299-304 (2011). DOI: https://doi.org/10.1016/j.phpro.2011.11.047
- [26] X.L. Zhong, M. Gupta, Development of lead-free Sn–0.7Cu/Al<sub>2</sub>O<sub>3</sub> nanocomposite solders with superior strength. J. Phys. D. Appl. Phy. 41 (9), 095403 (2008).
  DOI: https://doi.org/10.1088/0022-3727/41/9/095403
- [27] W. Yang, Y. Lv, X. Zhang, X. Wei, Y. Li, Y. Zhan, Influence of graphene nanosheets addition on the microstructure, wettability, and mechanical properties of Sn-0.7Cu solder alloy. J. Mater. Sci.-Mater. El. 31, 14035-14046 (2020). DOI: https://doi.org/10.1007/s10854-020-03920-8
- [28] Y. Lv, W. Yang, J. Mao, Y. Li, X. Zhang, Y. Zhan, Effect of graphene nano-sheets additions on the density, hardness, conductivity, and corrosion behavior of Sn–0.7Cu solder alloy. J. Mater. Sci.-Mater. El. 31, 202-211 (2020).
  DOI: https://doi.org/10.1007/s10854-019-02538-9

- [29] ASTM E3-11(2017), Standard Guide for Preparation of Metallographic Specimens, ASTM International, West Conshohocken, PA, 2017.
- [30] ASTM E407-07(2015)e1, Standard Practice for Microetching Metals and Alloys, ASTM International, West Conshohocken, PA, 2015.
- [31] M. Malaki, A. Fadaei Tehrani, B. Niroumand, M. Gupta, Wettability in metal matrix composites. Metals, 11(7), 1034 (2021).
  DOI: https://doi.org/10.3390/met11071034
- [32] N. Rodrigues, A.C. Ferreira, S.F. Teixeira, D. Soares, J.C. Teixeira, F. Cerqueira, F. Macedo, Contact angle measurement of SAC305 solder: numerical and experimental approach. J. Mater. Sci-Mater. El. 27, 8941-8950 (2016).
  DOI: https://doi.org/10.1007/s10854-016-4924-4
- [33] ASTM E384-10(2010), Standard test method for Knoop and Vickers hardness of materials, ASTM International, West Conshohocken, PA, 2010.
- [34] M. Zhao, L. Zhang, Z.Q. Liu, M.Y. Xiong, L. Sun, Structure and properties of Sn-Cu lead-free solders in electronics packaging. Sci. Technol. Adv. Mat. 20 (1), 421-444 (2019).
  DOI: https://doi.org/10.1080/14686996.2019.1591168
- [35] Y. Huang, Z. Xiu, G. Wu, Y. Tian, P. He, X. Gu, W. Long, Improving shear strength of Sn-3.0Ag-0.5Cu/Cu joints and suppressing intermetallic compounds layer growth by adding graphene nanosheets. Mater. Lett. 169, 262-264 (2016).
  DOI: https://doi.org/10.1016/j.matlet.2016.01.125
- [36] M.M. Salleh, A.M. Al Bakri, F. Somidin, A.V. Sandu, N. Saud, H. Kamaruddin, K. Nogita, A comparative study of solder properties of Sn-0.7Cu lead-free solder fabricated via the powder metallurgy and casting methods. Rev. Chim-Bucharest. 64 (7), 725-728 (2013).
- [37] L. Yin, Z. Zhang, Z. Su, C. Zuo, Z. Yao, G. Wang, Y. Zhang, Effects of graphene nanosheets on the wettability and mechanical properties of Sn-0.3Ag-0.7Cu lead-free solder. J. Electron. Mater. 49, 7394-7399 (2020).
  DOI: https://doi.org/10.1007/s11664-020-08537-5
- [38] D. Manasijević, L. Balanović, I. Marković, M. Gorgievski, U. Stamenković, A. Kovačević, Thermal properties and microstructure of Al–Sn alloys. J. Phys. Chem. Solids. 195, 112297 (2024). DOI: https://doi.org/10.1016/j.jpcs.2024.112297
- [39] X.D. Liu, Y.D. Han, H.Y. Jing, J. Wei, L.Y. Xu, Effect of graphene nanosheets reinforcement on the performance of Sn-Ag-Cu leadfree solder. Mat. Sci. Eng. A-Struct. 562, 25-32 (2013). DOI: https://doi.org/10.1016/j.msea.2012.10.079
- [40] M.L. Li, L.L. Gao, L. Zhang, N. Jiang, S.J. Zhong, L. Zhang, Interfacial reaction and properties of Sn/Cu solder reinforced with graphene nanosheets during solid—liquid diffusion and reflowing. J. Mater. Sci.-Mater. El. 32, 26666-26675 (2021). DOI: https://doi.org/10.1007/s10854-021-07044-5